Wave spectral energy variability in the northeast Pacific

Peter D. Bromirski

Integrative Oceanography Division, Scripps Institution of Oceanography, University of California, San Diego, La Jolla, California, USA

Daniel R. Cayan[1]

Climate Research Division, Scripps Institution of Oceanography, University of California, San Diego, La Jolla, California, USA

Reinhard E. Flick

California Department of Boating and Waterways, Integrative Oceanography Division, Scripps Institution of Oceanography, University of California, San Diego, La Jolla, California, USA

Received 23 March 2004; revised 13 October 2004; accepted 19 January 2005; published 8 March 2005.

[1] The dominant characteristics of wave energy variability in the eastern North Pacific are described from NOAA National Data Buoy Center (NDBC) buoy data collected from 1981 to 2003. Ten buoys at distributed locations were selected for comparison based on record duration and data continuity. Long-period (LP) [$T > 12$] s, intermediate-period [$6 \leq T \leq 12$] s, and short-period [$T < 6$] s wave spectral energy components are considered separately. Empirical orthogonal function (EOF) analyses of monthly wave energy anomalies reveal that all three wave energy components exhibit similar patterns of spatial variability. The dominant mode represents coherent heightened (or diminished) wave energy along the West Coast from Alaska to southern California, as indicated by composites of the 700 hPa height field. The second EOF mode reveals a distinct El Niño-Southern Oscillation (ENSO)-associated spatial distribution of wave energy, which occurs when the North Pacific storm track is extended unusually far south or has receded to the north. Monthly means and principal components (PCs) of wave energy levels indicate that the 1997–1998 El Niño winter had the highest basin-wide wave energy within this record, substantially higher than the 1982–1983 El Niño. An increasing trend in the dominant PC of LP wave energy suggests that storminess has increased in the northeast Pacific since 1980. This trend is emphasized at central eastern North Pacific locations. Patterns of storminess variability are consistent with increasing activity in the central North Pacific as well as the tendency for more extreme waves in the south during El Niño episodes and in the north during La Niña.

Citation: Bromirski, P. D., D. R. Cayan, and R. E. Flick (2005), Wave spectral energy variability in the northeast Pacific, *J. Geophys. Res.*, *110*, C03005, doi:10.1029/2004JC002398.

1. Introduction

[2] An integral component of the ocean climate of the eastern North Pacific is the spatial/temporal structure of surface gravity waves. The gravity wave field is a response to surface wind forcing, which is caused by synoptic-scale features but also varies over interannual and decadal timescales. Because long-period surface waves are most effectively generated by long fetches of wind, and because they may propagate hundreds or thousands of kilometers, the wave field is a result of both local and remote wind forcing. Thus the fluctuations in eastern North Pacific wave energy are a signature of climate variability not only over the immediate coastal region, but also from broader basin-scale atmospheric patterns.

[3] Storm waves damage and flood coastal facilities and structures, and are a dominant driving force for beach erosion [e.g., *Armstrong and Flick*, 1989]. Furthermore, different portions of the wave spectrum are implicated in different aspects of coastal impacts; for example, short-period waves deplete beach sands while longer-period waves with lower steepness transfer sands to beaches from offshore bars.

[4] Although it is sometimes affected by southern ocean swell, the eastern North Pacific is dominated by gravity waves from the North Pacific basin, especially during boreal winter when the Aleutian Low and other North Pacific

[1] Also at U.S. Geological Survey, La Jolla, California, USA.

0148-0227/05/2004JC002398$09.00

circulation patterns are most active. These circulation patterns vary greatly within and between individual winter seasons [*Namias*, 1968, 1978] and are known to respond to tropical climate influences [*Bjerknes*, 1966; *Horel and Wallace*, 1981; *Mo and Livezey*, 1986; *Nitta and Yamada*, 1989] and to perturbations in the extratropical westerly wind systems [*Namias*, 1968, 1978; *Dole*, 1986].

[5] The evidence from direct or inferred observations of ocean surface waves in the eastern North Pacific indicates that particular winters or series of winters produce extraordinarily high wave activity while others do not [*Inman and Masters*, 1991]. Recently, *Allan and Komar* [2000] presented evidence suggesting an increasing trend in wave heights off the Washington/Oregon coast, consistent with upward trends since about 1950 in North Pacific storm activity [*Graham and Diaz*, 2001] and in a San Francisco tide gauge storminess index [*Bromirski et al.*, 2003].

[6] This study employs time series of wave spectral energy from a set of NOAA National Data Buoy Center (NDBC) eastern North Pacific buoys to investigate the patterns and temporal changes of the winter wave field during the period since 1981. Although this time period is not long enough to capture changes that occurred in North Pacific climate during the mid-1970s, it does include the massive El Niño events of 1982–1983 and 1997–1998 as well as La Niña events and other important Pacific climate fluctuations. Questions we seek to answer include the following. (1) Are there regional or larger modes of spatial variability of winter wave energy? (2) How has wave energy varied over time? In particular, is wave energy variability linked to Pacific climate patterns such as El Niño-Southern Oscillation (ENSO)? (3) Do short-, intermediate-, and long-period wave energy components vary independently? These questions are addressed by comparison of residuals of wave parameters using empirical orthogonal functions (EOFs) to estimate spatial relationships of the wave energy distribution. The dominant EOFs and their associated principal components (PCs), together with the occurrence and distribution of monthly wave parameter and residual extremes, are used to identify features of the spatial and temporal variability of the northeast Pacific wave field.

2. NE Pacific Buoy Data

[7] Continuous hourly nondirectional wave measurements [*Steele et al.*, 1985] along the Pacific coast of North America were initiated by NOAA during the early 1980s. Ten NOAA buoys at distributed locations in the northeast (NE) Pacific (Figure 1) were selected for comparison of wave climate parameters covering the 1981–2003 period. Buoy selection was based on data continuity, duration, and location.

[8] The processing methodology of the fixed hull accelerometer data from NOAA buoys was changed in June 1984. The processing change has the greatest impact on spectral estimates at frequencies less than about 0.09 Hz, causing the more recent data to have higher energy at longer periods. Because the difference in long-period energy due to the processing change is greatest during low-amplitude swell-dominated seas [*Earle et al.*, 1984], winter monthly means, that are dominated by high-amplitude storm events

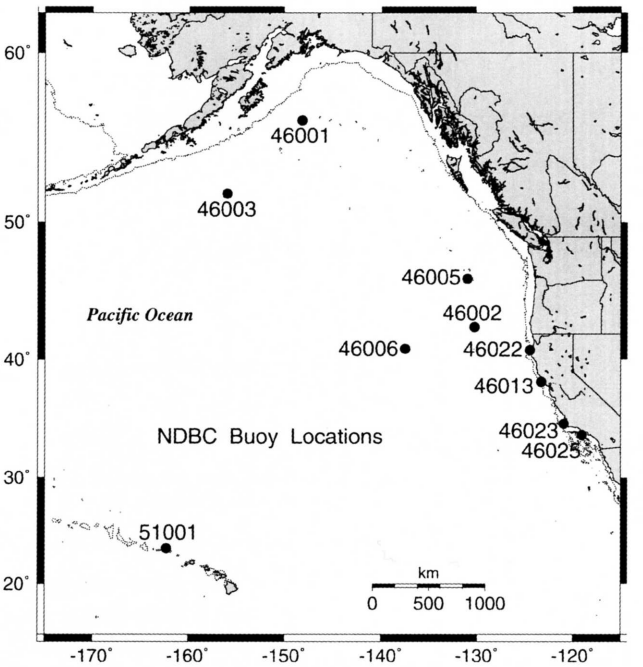

Figure 1. Locations of the primary NOAA buoys (solid circles) in this study. The bathymetric contour (light line) is at 1000 m depth.

and used in our analyses below, are thought to be only minimally affected. However, because the raw data were not archived and thus the earlier data cannot be reprocessed, there is some uncertainty in the magnitude of the impact of the processing change on wave spectral estimates at wave periods greater than 10 s.

[9] The buoy data collection has not been continuous, with each buoy experiencing more than a few periods of varying length of nonoperation. Buoy 46003's mooring became loose during January 1999, and its operation was subsequently discontinued. Data from nearby buoy 46066 is substituted for 46003 from May 2000 to the present. Several data gaps at buoys 46013 and 46023 are filled with data from nearby buoys 46014 and 46011, respectively. Significant wave height correlations between these buoy pairs during periods of common operation yield $\mathcal{R}^2 \approx 0.9$ during winter months. Locations of these auxiliary buoys can be found at the NDBC Web site (http://www.ndbc.noaa.gov).

3. Seasonal Wave Climate

[10] The wave climate consists of "sea" generated by local winds as well as swell propagating from distant storms. The significant wave height, (H_s, approximately the average of the highest 1/3 of the waves) and mean wave period, T_m, include contributions from both sea and swell. Although H_s is commonly used to describe wave climate variation, wave spectral density data provide significantly more information by allowing some differentiation between distant and local wave generation. The short-period (SP) portion of the wave spectrum, i.e., wave period, $T < 6$ s, is dominated by local seas, while the long-period (LP) portion, $T > 12$ s, results primarily from swell. Intermediate-period (IP) wave energy, $6 \text{ s} \leq T \leq 12$ s, probably results from a

mixture of local and regional wind forcing. Variations in wave energy at different buoys for the same storm event result from their proximity to the strong wind sector of a storm, fetch parameters, and wavefront spreading, although bottom interaction in relatively shallow coastal waters causing refraction and shoaling can also be important. Because high-amplitude LP waves are generated only by high sustained wind speed over a large fetch, the variation and distribution of LP wave energy in the NE Pacific gives a measure of extreme storm characteristics. In addition, because wavefront spreading and dissipation from wave breaking cause a more rapid reduction in short-period wave energy away from the generation region, the variation in SP wave energy at a given buoy during winter months probably reflects heightened local-to-regional storm activity.

[11] The variation of the wave climate can be described by several measures from the hourly buoy estimates of wave parameters. Pronounced differences on synoptic timescales are observed between buoys, demonstrating the importance of storm location, fetch, wind speed and direction on the local wave climate. Because of the large synoptic variability in wave energy throughout the NE Pacific, monthly means provide a useful comparison between widely separated locations, giving sufficient temporal resolution of both intraseasonal and interannual variability. The occurrence of extrema in LP, IP, and SP wave energy, their distribution in the NE Pacific, and their temporal variation give additional important information about potential wave climate changes and trends.

[12] The long-term monthly means for all months having at least 85% of possible hourly measurements are used to establish reference levels of the wave climate parameters at each buoy. The parameters investigated in this study include band-limited wave energy estimates, obtained by summing the wave spectral energy in selected bands, the mean wave period, T_m, and the wind speed, W_s.

[13] Hourly band-limited wave energy estimates were determined for the SP, IP, and LP bands. Long-term monthly means of these parameters (Figure 2) show a general decrease from north to south, with the seasonal peaks for LP and IP wave energy commonly in December. The coastal stations (buoys 46022, 46013, and 46023) have higher average LP energy during winter months compared with IP energy, indicating swell dominance, while the opposite is true for deep water open-ocean buoys where IP energy generally dominates throughout the year. Buoy 46025 in the southern California Bight is shielded from waves propagating from storm centers to the northwest by Pt. Conception and the Channel Islands. The resulting band-limited wave energy long-term monthly means at 46025 in the LP and IP bands (not shown) are substantially lower (about 35% of nearby buoy 46023). However, the dominant portion of LP and IP wave energy observed at 46025 is generated primarily in the open ocean and thus reflects open ocean wave variability.

[14] The seasonal patterns of variability of W_s (Figure 3) are more similar to those of IP and SP energy than LP energy, reflecting the importance of local to regional wind conditions in producing the shorter-period wave energy. Note the substantial seasonal variation in the amplitudes and variability of W_s at the coastal stations, strongly influenced by alongshore weather patterns during summer

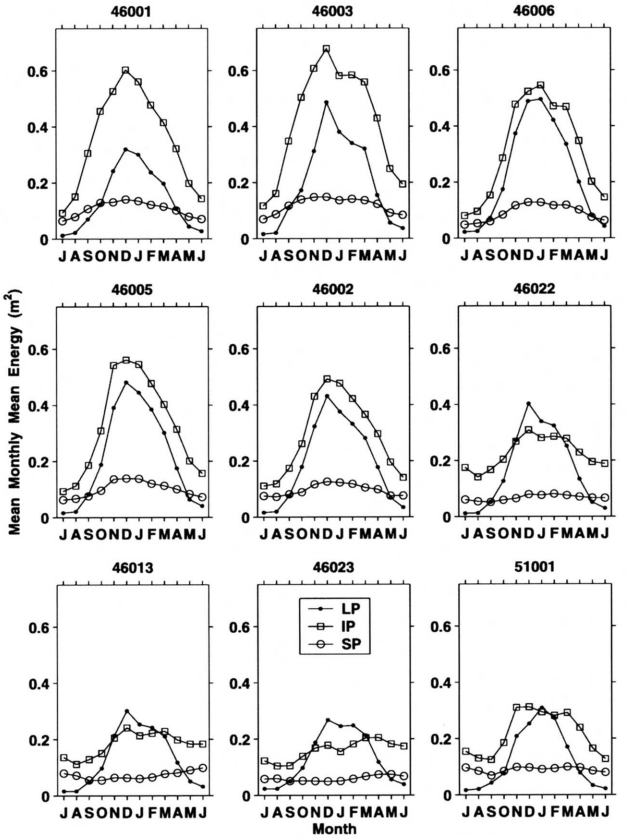

Figure 2. Band-limited wave energy seasonal means in short-period (SP) [$T < 6$] s, intermediate-period (IP) [$6 \leq T \leq 12$] s, and long-period (LP) [$T > 12$] s bands for all months having at least 85% of possible hourly measurements for buoys at locations shown in Figure 1.

months, while Hawaii buoy 51001 has a strong trade wind influence. In contrast, patterns of variability of T_m generally follow that of the dominant energy component, e.g., LP energy at the coastal buoys and IP energy at deep ocean buoys. Although SP energy generally comprises a small percentage of the total wave energy spectrum during major storm events, elevated winter SP monthly energy levels are an indicator of heightened winds from relatively local storminess.

[15] As would be expected, the seasonal patterns of variability of H_s (not shown), determined from the zeroth moment, m_0, of the full wave energy spectrum as $H_s = 4\ m_0^{1/2}$, generally follow the seasonal variability of the dominant wave energy component at respective buoys in Figure 2.

4. Monthly Variability

[16] How has the wave climate varied over the northeast Pacific since 1980? How do wave energy levels during the 1982–1983 El Niño compare with those during the 1997–1998 El Niño? These questions are addressed by comparison of monthly mean wave energy levels between three widely separated buoys. Monthly energy variability from the northern to the southern regions of the West Coast is demonstrated in Figure 4 for buoys 46003, 46005, and 46023 (see Figure 1 for locations), selected for detailed

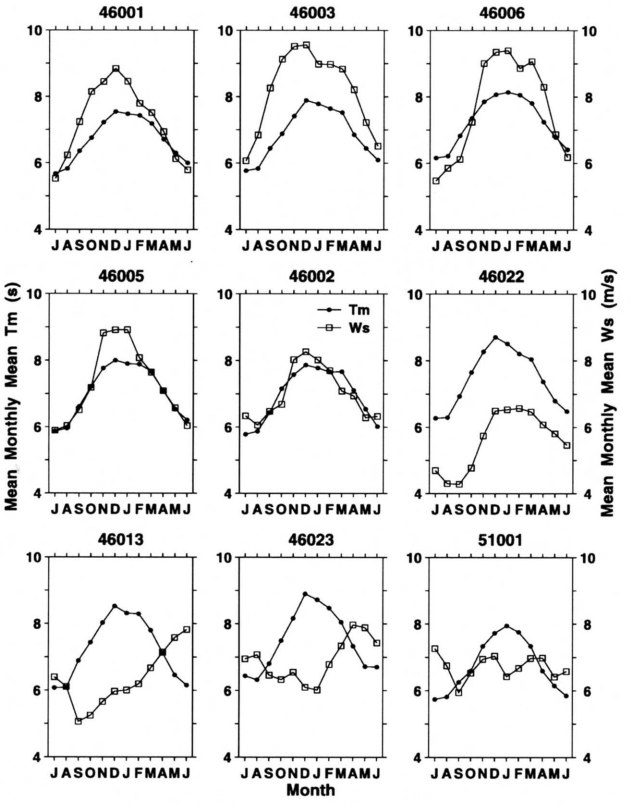

Figure 3. Mean wave period (full band), T_m (solid circles), and wind speed, W_s (squares), seasonal means for all months having at least 85% of possible hourly measurements at the buoys in Figure 2. Note the substantial difference in wind variability at buoys 46013, 46023, and 51001.

comparison because of their representative locations. Associated anomalies of monthly wave energy (Figure 5) are obtained as the difference between monthly energy levels and their respective long-term means shown in Figure 2, suggesting substantial long-period variability in wave energy across the North Pacific. Relative amplitude comparison of energy levels and their associated anomalies between widely separated buoys provides an indication of shifts in the dominant winter storm track paths as well as changes in average storm intensity.

[17] Elevated monthly energy levels can result from either a single extreme event or from a series of strong events having similar storm tracks. Elevated wave energy anomalies are generally expected at more northern buoys during La Niña episodes and at more southern buoys during El Niños (see Figure 14 below), and as estimated from other responses to intense storminess such as high precipitation and streamflow events [*Cayan et al.*, 1999]. Changes in wave energy at particular buoys can result from a persistent shift in proximity or orientation of storm activity, as well as from changes in storm intensity. For this reason there is some ambiguity whether changes in the levels of monthly means result primarily from changes in storm intensity or location (storm track shifts), or from a combination of both.

[18] The strong El Niños, 1982–1983 and 1997–1998, produced massive storminess in the NE Pacific [*Hoerling and Kumar*, 2002] and very high wave heights along the Pacific coast [*Seymour*, 1996; *Allan and Komar*, 2000]. The highest monthly LP levels in the 1980–2003 period observed at 46005 and 46023 (and at other buoys not shown) occurred during February 1998, during the mature phase of the 1997–1998 El Niño episode, with LP levels substantially higher than during the peak phase of the 1982–1983 El Niño. These most extreme monthly LP levels observed at widely separate locations suggest that atmospheric circulation patterns during the 1997–1998 El Niño produced the most intense winter storm waves throughout the NE Pacific recorded in the present data set. At Aleutian buoy 46003, the LP energy anomalies were small during both great El Niños (Figure 5), consistent with more southerly storm activity during these episodes. Note that LP energy levels and their anomalies at 46023 during the 1982–1983 El Niño were not exceptionally high. In contrast, SP energy at 46023 was substantially higher during the 1982–1983 winter than the 1997–1998 El Niño, indicating that 1982–1983 storms tracked much further south than normal and maintained high winds as they approached the coast. Extreme SP wave events were particularly numerous during 1982–1983 along the southern California coast, illustrated

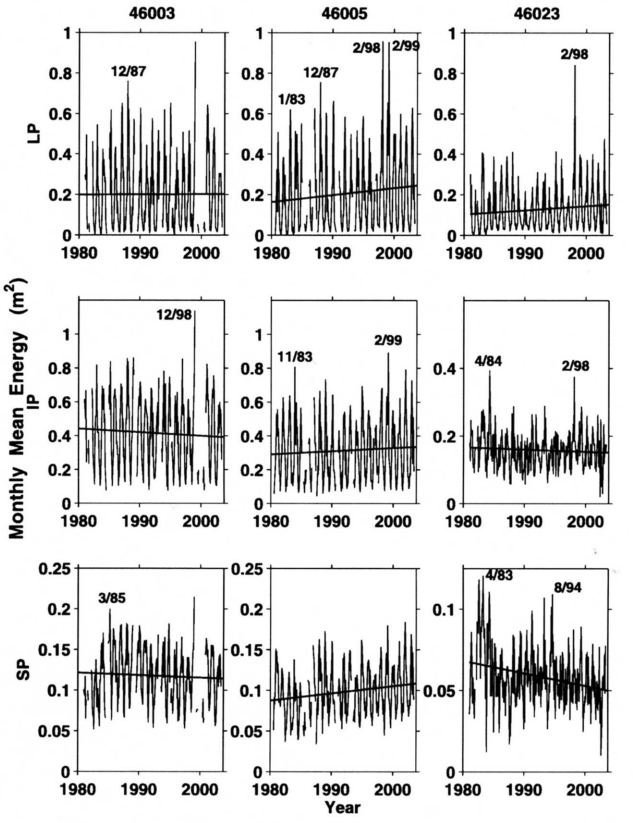

Figure 4. Mean monthly wave energy at buoys 46003, 46005, and 46023 (see Figure 1 for locations) in the LP, IP, and SP bands. Note that the vertical axis for the IP and SP bands at 46023 is half that of 46003 and 46005. Winter months from 1999 to 2002 are missing at buoy 46003 and during 1985–1986 at 46005. Solid lines are least squares trends. Annotated dates identify the highest nearby extremes.

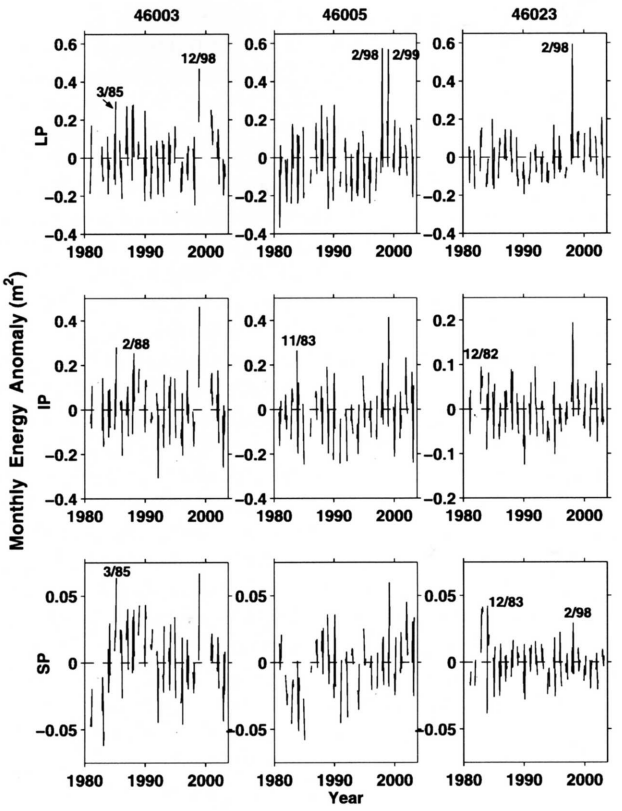

Figure 5. Monthly wave energy anomalies at buoys 46003, 46005, and 46023 (see Figure 1 for locations) in the LP, IP, and SP bands. Note that the vertical axis for the IP band at 46023 is half that of 46003 and 46005. Only winter months (November–March) having at least 85% of available data are shown. Annotated dates signify the month of the highest peaks.

in Figure 14 below. Together, the LP and SP levels observed along the eastern North Pacific buoy network indicate that the storms during the 1997–1998 El Niño produced higher waves than those during 1982–1983; that is, storms were either larger and/or had higher sustained winds, but the 1997–1998 storms took more northerly tracks.

[19] The effects of altered storminess during La Niña is evident from LP wave energy variations. The highest monthly LP energy at 46003 occurred during December 1998, a moderately strong La Niña, with concurrent maxima for both IP and SP energy. Similarly, high monthly LP energy levels occurred at 46005 during the 1998–1999 winter (the winter following the 2/98 extreme in Figure 5), with only moderate LP levels at southernmost buoy 46023 as indicated by the small positive monthly energy anomaly at 46023 during winter 1998–1999 (Figure 5). Similar wave energy fluctuations are observed across the northeast Pacific during the 1988–1989 and 1999–2000 La Niñas. These observations yield a consistent pattern of northerly displaced storminess and heightened wave energy during La Niña. This northward shift is further corroborated by 700 hPa height anomaly composites (see Figure 11 below).

[20] Upward trends in LP energy levels are observed at buoys 46005 (offshore Washington) and 46023 (near Pt. Conception) in Figure 4 (and at buoys 46006 and 46002, not shown). These trends most likely result from increasing storm intensity. The increasing trend in LP energy at 46023, coupled with a decreasing trend in SP energy at 46023, is consistent with increasing storm intensity at distant locations.

[21] Decreasing trends of IP and SP energy at both 46003 and 46023, coupled with an increasing trend in SP energy at 46005 (Figure 4), suggest a progressive shift in storm activity to the central latitudes of the eastern North Pacific, and/or an increase in storm intensity near 46005, both of which would tend to cause an increasing trend in average wave heights at 46005. Decreasing trends in W_s at 46003 and 46023 (Figure 6) are consistent with reduced local storm activity near these locations. These trends in wave climate parameters are consistent with a concentration of storm activity across the central North Pacific (see Figure 13 below), in general agreement with increasing frequency and intensity of cyclones between 25° and 40° [*Graham and Diaz*, 2001].

[22] The apparent extreme southern displacement of storm activity during the 1982–1983 El Niño, resulting in comparatively low wave energy levels in the north, may significantly influence trend analyses at more northern locations such as 46005. Note also that, because of its north central location offshore Washington, 46005 is exposed to significant wave energy generated during both El Niño and La Niña episodes, e.g., 1997–1998 and 1998–1999. Thus increasing trends in LP energy (Figure 4) and H_s at 46005 [*Allan and Komar*, 2000] are a consequence of waves forced by atmospheric circulation patterns associated with both of these modes. In contrast, extreme positive monthly anomalies at 46003 occur almost exclusively during La Niña episodes, while extremes at 46023 are more likely during El Niños.

5. Spatial Structure

[23] The broad-scale spatial variation of wave energy can be estimated from EOFs of the band-limited monthly energy

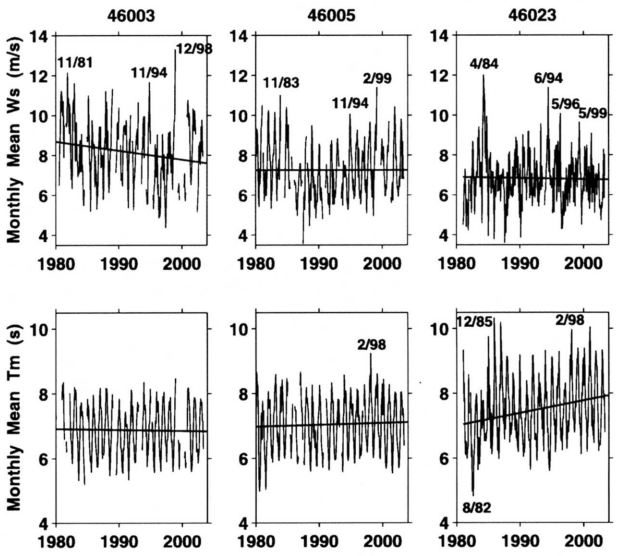

Figure 6. Mean monthly wind speed, W_s, and mean wave period, T_m, at buoys 46003, 46005, and 46023 (see Figure 1 for locations). Solid lines are least squares trends.

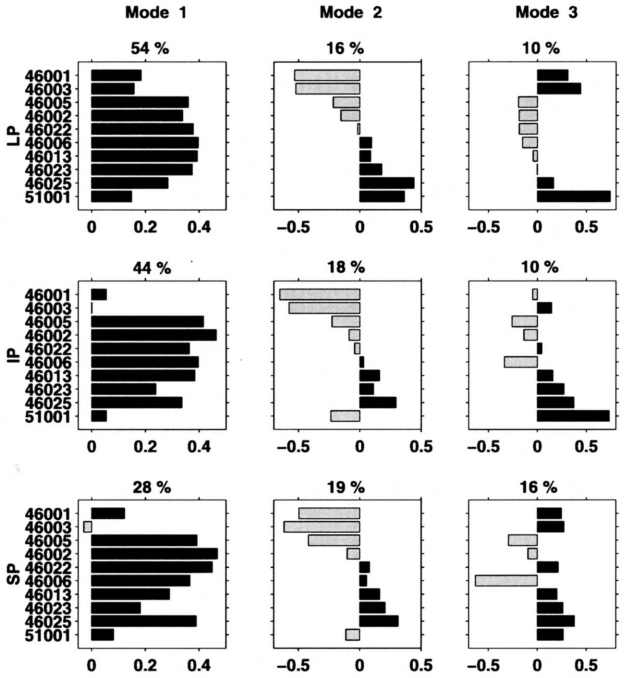

Figure 7. Empirical orthogonal functions (EOFs) of the first three modes for LP, IP, and SP determined for winter (November–March) monthly energy anomalies at the ten buoys shown in Figure 1, arranged from north to south. The percent of the variance explained by each mode is shown above each subplot. The long-term monthly mean anomalies at respective buoys were substituted for missing data. The total variances explained by the first three LP, IP, and SP modes are 80%, 72%, and 63%, respectively.

anomalies, each normalized to unit variance. We restrict our analysis to winter months (November–March) to exclude seasonal variability related to longshore winds at near-coastal buoys and strong trade wind components near Hawaii, and to concentrate on the peak boreal storm period.

[24] The first, most important EOF is a mode having most stations from Alaska to southern California covarying for each of the three frequency bands (Figure 7). The first mode represents the dominance of atmospheric circulation patterns that produce anomalously high (or low) wind patterns that force waves across most of the NE Pacific basin. EOF 2 has a distinct north-south expression that again occurs for each frequency band. From results described above that compared anomalous wave energy across the respective buoys, EOF 2 is likely associated with ENSO-related forcing that causes above normal wave energy at southern locations during El Niño and above normal wave energy at northern locations during La Niña. LP EOF 3 has a stronger northern expression than LP EOF 2, and is consistent with more northern storm tracks.

[25] The fraction of the variance explained by EOF 1 of the SP energy (28%) is about half that of EOF 1 of LP energy (54%). This contrast may be explained by the fact that high LP waves are only generated by large-scale wind systems that have a broad-scale impact throughout the NE Pacific basin, whereas high SP waves can be produced by more regional and more coastal wind disturbances. For example, comparison of LP energy from Hawaii buoy 51001 with California coastal buoys 46022, 46013, and 46023 indicates that there is a high correlation ($\mathcal{R} > 0.7$) of monthly levels of LP energy between the two locales, even though they are separated by about 3000 km. In fact, inspection of the hourly wave spectra from these sites reveals that swell from the same storm recorded north of the Hawaiian chain may appear at the California coast a few days afterward. Similar analyses yield less correlation for IP wave energy and low correlation across SP wave energy between Hawaii and California sites. This also indicates that SP energy levels are much more closely tuned to local-to-regional changes in storm activity than are LP levels. Note that for SP EOF 3, all near-coastal buoys at California have the opposite phase of the open ocean buoys, also indicative of the importance of local SP generation.

[26] Confirming the results from individual buoys discussed above, the PC amplitudes associated with dominant EOF mode 1 (Figure 8) indicate that the 1997–1998 El Niño produced the wave energy levels over the eastern North Pacific basin more than 50% higher than any other winter since 1980. Furthermore, from the NE Pacific perspective, the 1997–1998 winter wave energy levels were substantially higher than those during the 1982–1983 El Niño. The large difference in wave energy between the 1982–1983 and 1997–1998 winters shows that even the strongest El Niños produce widely variable wave energy levels, consistent with studies demonstrating that a signif-

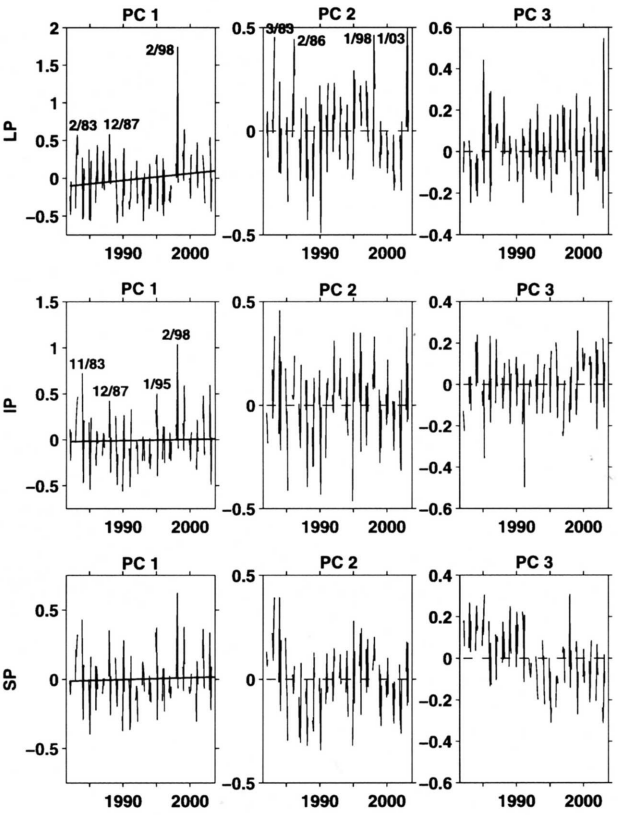

Figure 8. Principal components of LP, IP, and SP winter (November–March) monthly energy anomalies associated with the first three EOF modes in Figure 7. Solid lines for PC1 are least squares fits, while PC2 and PC3 have zero lines dashed. Some extremes are identified for reference.

icant part of the North Pacific atmospheric response is sensitive to warming in the tropical Pacific [e.g., *Gershunov and Barnett*, 1998; *Hoerling and Kumar*, 2002].

6. Correlations Across Frequency Bands

[27] Although individual storms and resulting synoptic extremes undoubtedly influence the monthly anomalies, the wave energy records are sufficiently long to obtain a reasonable estimate of wave variability. The distribution of buoys used in these analyses is clearly not uniform and does not cover as much of the NE Pacific as would be desired. However, because LP waves propagate with little attenuation in deep water, LP energy from large, remote cyclonic systems has nearly a basin-wide impact. On the other hand, IP and SP variability are more sensitive to local-to-regional storm activity. Because IP and SP energy observed simultaneously at individual buoys are usually generated by the same storm systems, correlations of hourly data between these two frequency components at the same open ocean buoy during individual winter months are high, yielding correlation coefficients, $\mathcal{R}$, of about 0.75 (not shown). The IP and SP correlations are significantly higher than correlations between LP and SP energy at the same buoy, which have $\mathcal{R} \approx 0.4$. At buoy locations along the southern California coast and near Hawaii, correlations between LP and SP energy can be considerably lower. However, for EOFs 1 and 2, the PC time series for each of the frequency bands is well correlated with the others (Table 1), indicating that variations of the same large-scale wind forcing dominates the surface wave spectrum contemporaneously throughout the NE Pacific. Thus it is not surprising that gravity wave trains from the same storm system, considering propagation lags, can be observed both at Hawaii and along the California coast.

[28] Correlations of wave energy principal components with each other (Table 1) show that the IP and SP bands are more closely related than either LP and IP or LP and SP bands, probably reflecting that much of the LP energy has a broader and more distant generation area, and thus confirming the sensitivity of the shorter-period bands to regionally forced wave energy. The broad-scale significance of the EOF/PC results can be demonstrated from 700 hPa height anomaly composites obtained for principal component (PC) extremes, and by correlations of the PCs with broad-scale climate indices.

7. Atmospheric Circulation

[29] The relationship of winter energy variability to Northern Hemisphere atmospheric circulation patterns is determined from 700 hPa height monthly anomaly composites determined for winter months containing high and low PC extremes for modes 1 and 2 for the LP, IP, and SP bands. These anomalies were mapped over a 5° latitude × 10° longitude Northern Hemisphere grid. The statistical significance of each location's composite anomaly was judged via a null hypothesis by gauging against the overall mean anomaly (zero) using a two-tailed t-test. Each month was considered to be an independent sample in calculating degrees of freedom. Composite anomaly maps were generated using 700 hPa height data for the set of months whose PC amplitudes were amongst the 10 highest, and 10 lowest, respectively. Grid locations whose composite anomaly is significantly different from the null hypothesis at ≥95% confidence were identified.

Table 1. Correlation Coefficients, $\mathcal{R}$, of Winter (November–March) Band Energy Principal Components: Long-Period (LP) Versus Intermediate-Period (IP), LP Versus Short-Period (SP), and IP Versus SP for Common Modes[a]

Band	Mode	IP (p)	SP (p)
LP	1	**0.77** (0.00)	**0.68** (0.00)
	2	**0.82** (0.00)	**0.73** (0.00)
	3	0.24 (0.29)	−0.17 (0.46)
IP	1		**0.92** (0.00)
	2		**0.85** (0.00)
	3		**0.47** (0.03)

[a]Principal components are shown in Figure 8. Values in parentheses, p, associated with the preceding $\mathcal{R}$, are t-test-derived probabilities, assuming that the data are normally distributed; p values < 0.05 indicate that the associated $\mathcal{R}$ (in boldface) is statistically significant.

[30] The contrast between composites for PC extremes is most pronounced for IP PC mode 1 (PC1, Figure 9). Two distinct anomaly patterns for (1) high and (2) low PC extremes emerge: (1) a broad region of highly significant negative anomalies across middle latitudes of the central and eastern North Pacific extending southward to about 30°N and (2) a region of highly significant positive anomalies centered over the eastern Gulf of Alaska. The high winter IP PC1 composite features the intensified and southerly displaced Aleutian Low that is characteristic of the PNA atmospheric circulation pattern [*Wallace and Gutzler*, 1981; *Barnston and Livezey*, 1987]. The positive phase of the PNA, consists of a deep, accentuated low south of the Aleutian Islands with a high-pressure ridge over western North America. This deep low, coupled with significant positive anomalies over north central and eastern Canada, is associated with a swath of storms traveling from British Columbia southward to California. The deep low distribution shown in the high winter IP PC1 composite would result in intense storm activity both in the Pacific Northwest and along the California coast, as evidenced by monthly mean wave energy and associated anomalies at both 46005 in the north and 46023 in the south during the 1997–1998 El Niño winter (Figures 4 and 5). Also, the high IP PC1 pattern is similar to that obtained by *Bromirski et al.* [2003] for extreme storminess along the West Coast determined from tide gauge data at San Francisco. In contrast, the low winter IP PC1 composite shows an accentuated West Coast high-pressure ridge, with a relatively weak but significant low over the central North Pacific, resulting in low storm activity and low wave energy in the NE Pacific. To understand differences in storm activity associated with these atmospheric circulation patterns, we have also examined 500 hPa height variability (see Figure 13 below).

[31] Composites for high and low LP PC1 extremes (Figure 10) show the significant anomaly patterns shifted to the west compared with counterparts IP and SP PC1 (Figure 9). The more western-accentuated high LP PC1 pattern is consistent with the requirement that long-period waves have a basin-scale wind system. As in the IP PC1 case, this pattern resembles the circulation associated with the deep Aleutian Low phase of the PNA [*Barnston and*

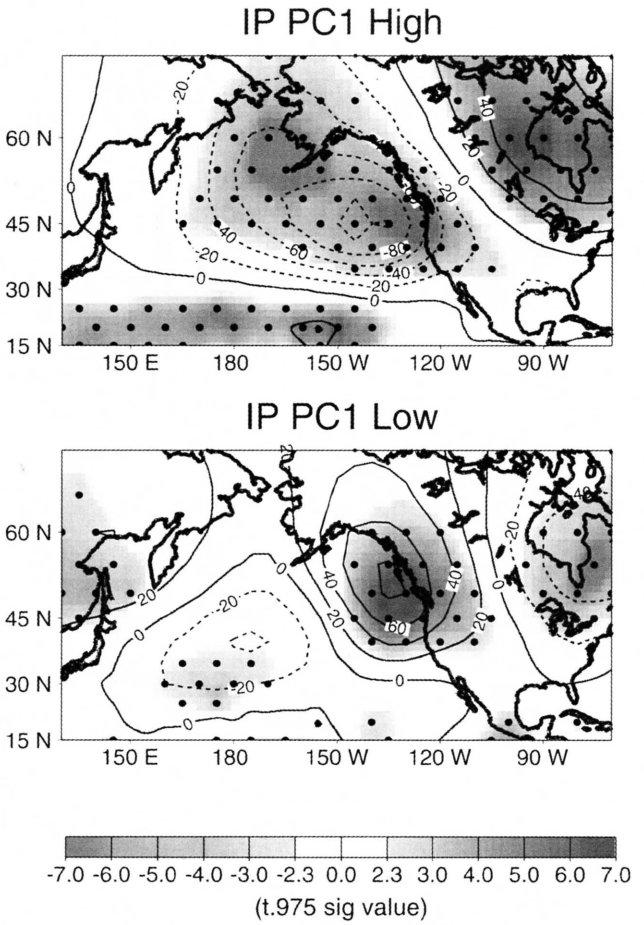

Figure 9. Composite 700 hPa height anomalies for months with the (top) 10 highest and the (bottom) 10 lowest IP principle component (PC) mode 1 extremes (see Figure 8). Statistically significant negative anomalies are blue, and statistically significant positive anomalies are red. See color version of this figure at back of this issue.

Livezey, 1987] or the North Pacific Index (NPI [*Trenberth and Hurrell*, 1994]). As would be expected from the high correlations between IP and SP EOF 1 (Table 1), the 700 hPa composite patterns for SP PC1 more closely resemble those of IP PC1 than LP PC1. This is consistent with IP and SP being more closely associated with regional-to-local storminess than LP.

[32] Composites of 700 hPa anomalies obtained for the highest and lowest PC cases from EOF 2 (Figure 11) produce anomalous patterns that resemble the Northern Hemisphere atmospheric circulation's response to ENSO [*Bjerknes*, 1969; *Namias*, 1976; *Mo and Livezey*, 1986]. North Pacific 700 hPa height anomalies composited for high LP PCs associated with EOF mode 2 reveal an El Niño-like atmospheric pattern, with an intense low shifted to the south driving waves toward the California coast (Figure 11). In comparison to the high LP PC1 composite, the pattern associated with high LP PC2 levels has a more southerly displaced low, whose strong negative anomalies that extend to about 30N, characteristic of El Niño. Conversely, the low PC2 composite in Figure 11 exhibits a relatively strong low centered near the Gulf of Alaska, characteristic of La Niña. Relatively strong correlations are found between PC2 of LP, IP, and SP and the Southern Oscillation Index (SOI), a prominent ENSO index that gives a measure of tropical atmospheric circulation, as shown in Table 2 and discussed below. The low LP PC2 circulation pattern would result in higher wave energy in the Gulf of Alaska and relatively low wave energy along the California coast. The more northerly negative anomalies along the northern edge of the Aleutian Islands (Figure 11, low LP PC2) are not as intense as that for high LP PC2, suggesting that atmospheric patterns associated with La Niña are not as strongly expressed as those for El Niño.

[33] The 700 hPa height anomaly composite associated with high SP PC2 levels (Figure 11) shows highly significant negative anomalies that are much more zonally constrained than high LP PC2. This zonal pattern is consistent with heightened storm activity in the southern and central midlatitudes of the northeast Pacific, identified from a general decrease in mean monthly IP and SP wave energy since the early 1980s (see Figure 4 above). The low SP PC2 700 hPa height anomaly composite is similar to low LP SP2, again favorable for producing higher wave energy to the north. The distinct contrast between atmospheric circulation patterns associated with high versus low PC extremes demonstrates the broad-scale forcing of the anomalous coastal wave climate, and also demonstrates that wave energy variability can serve as an indicator of winter storminess over extensive regions of the North Pacific and western North America.

8. Associations With Large-Scale Climate Indices

[34] The relationship of the LP, IP, and SP wave energy modes to atmospheric circulation patterns can be estimated by correlations of their principal components with broad-scale climate indices, such as the SOI and PNA [*Wallace and Gutzler*, 1981]. Correlations with the NPI [*Trenberth and Hurrell*, 1994] are similar to those with PNA, so they are not shown here. To correspond to cumulative winter PCs, demeaned, normalized cumulative winter (November–March) values of the SOI and PNA were obtained (Figure 12). These show coincident, pronounced peaks during the 1982–1983 and 1997–1998 El Niños when extreme storm conditions prevailed in the northeast Pacific. Wave energy PCs that result in high correlation coefficients with these indices (Table 2) have corresponding peaks during these extreme winters, showing the covariability of winter wave conditions with the SOI and PNA in the northeast Pacific.

[35] Correlations show that overall, the PNA has the strongest influence upon wave energy in the northeast Pacific (Table 2). Highly significant, relatively high correlations are observed between PNA and EOF 1 of all frequency bands. These correlations indicate that when the PNA is in its "deepened Alaskan low" phase, wave energy is increased for all three frequency bands along most of the eastern North Pacific, a result of the broad-scale anomalous wind field. Conversely, the opposite, weak Aleutian Low phase of PNA results in reduced wave energy across the region. The association of anomalous wave energy with ENSO (SOI) has a more regional structure than that with PNA. While the SOI is poorly correlated with EOF 1 for all

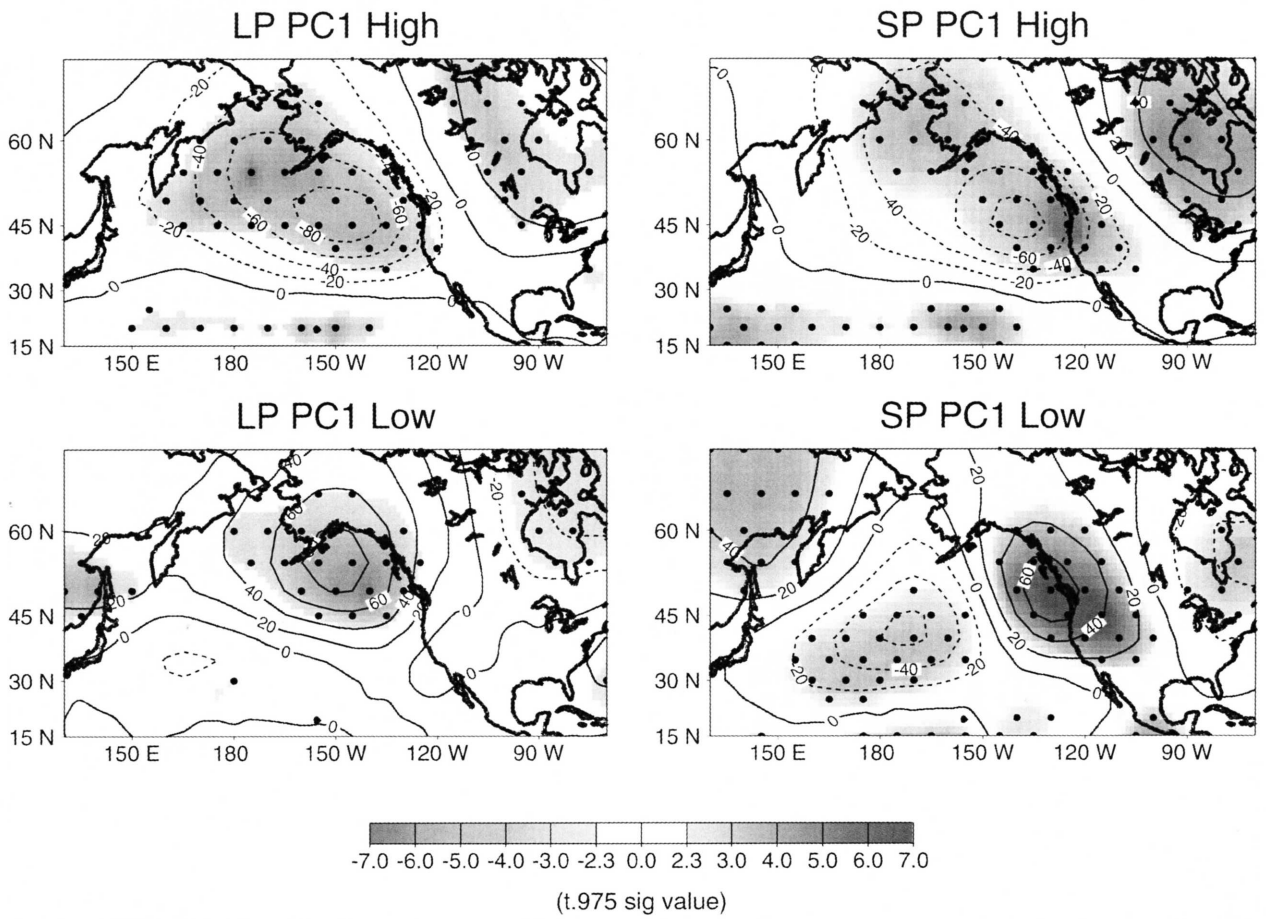

Figure 10. Composite 700 hPa height anomalies for months with the (top) 10 highest and the (bottom) 10 lowest (left) LP and (right) SP principle component (PC) mode 1 extremes (see Figure 8). Statistically significant negative anomalies are blue, and statistically significant positive anomalies are red. See color version of this figure at back of this issue.

bands, relatively high, significant correlations are obtained between the SOI and EOF 2 for all wave energy bands. This is consistent with both extreme low LP and low SP PC2 700 hPa height anomaly composites (Figure 11), indicating ENSO produces a north-south shift in atmospheric circulation and thus a north-south shift in wave energy, as indicated by the EOF 2 structure in Figure 7.

[36] Changes in forcing associated with Pacific decadal variability (the Pacific Decadal Oscillation (PDO) [*Mantua et al.*, 1997]; the North Pacific Oscillation (NPO) [*Gershunov and Barnett*, 1998]) undoubtedly affect North Pacific atmospheric circulation patterns. However, most likely because the PDO (and NPO) has strong interdecadal variability and the buoy record is relatively short, poor correlations of the PDO with wave energy PCs were obtained for all bands and all modes, and are not included in Table 2.

[37] As implied by wave energy PC associations with the PNA and SOI (Table 2), the wave energy at some of the buoys must also be well correlated with these climate indices. Correlations of LP and SP winter wave energy anomalies with the PNA are, in general, much better than with the SOI (Table 3). The phase relationships of the correlations generally follow those indicated by the EOFs (Figure 7). Correlations of the PNA with LP energy at the three northernmost buoys, 46001, 46003, and 46005, are poor, emphasizing the north-south pattern of the wave energy distribution and the importance of El Niño-related atmospheric circulation patterns over the eastern North Pacific. Surprisingly poor correlations are consistently observed at buoy 46005, perhaps because its location is subject to wave energy from both El Niño and La Niña. Interestingly, SP energy and PNA are poorly correlated except at the two westernmost buoys, 51001 and 46003. Correlations of the PCs with the NPI are very similar to those with the PNA. Correlations with the SOI are generally poor, except for buoys 46003 and 46025, whose out of phase relationship is consistent with EOF SP mode 2 (Figure 7). The significant correlations of SP wave energy with SOI at 46025 (and 46023) emphasizes the importance of El Niño on SP wave and, by inference, wind conditions along the southern California coast.

[38] Correlation of cumulative winter LP anomalies at Hawaii buoy 51001 with the other buoys in this study shows the two northernmost buoys, 46001 and 46003, to be weakly correlated and out of phase with 51001. However, correlations with the other buoys are in phase and generally increase southward. Significant correlations ($\mathcal{R} > 0.45$, $p \leq 0.03$) are observed between LP anomalies

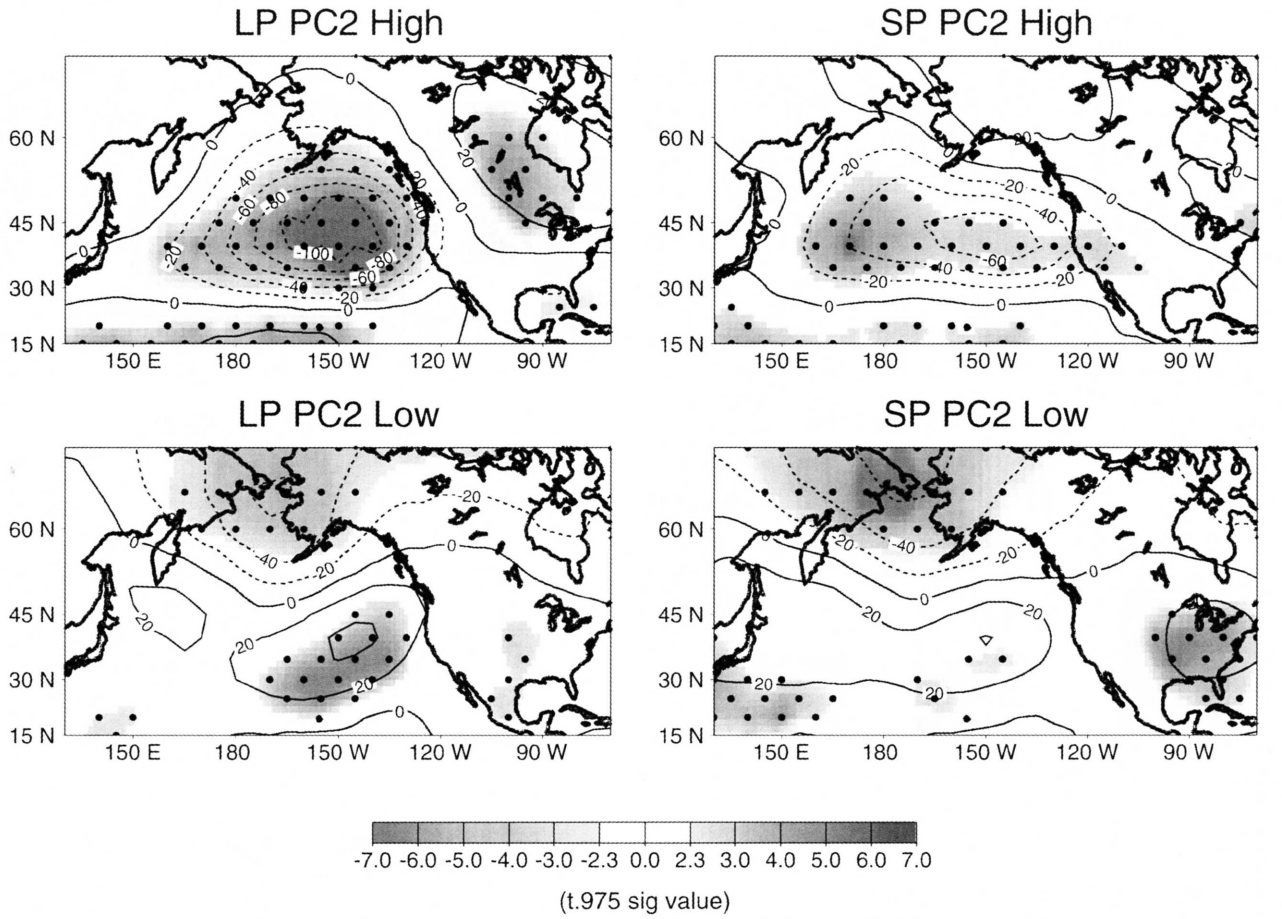

Figure 11. Composite 700 hPa height anomalies for months with the (top) 10 highest and the (bottom) 10 lowest (left) LP and (right) SP principle component (PC) mode 2 extremes (see Figure 8). Statistically significant negative anomalies are blue, and statistically significant positive anomalies are red. See color version of this figure at back of this issue.

at 51001 and buoys 46006, 46013, 46023, and 46025, indicating that related storm systems and possibly the same long-period waves that affect Hawaii affect the wave climate of southern California. In contrast, all correlations of cumulative winter SP anomalies at 51001 with the other buoys are poor and not significant, not surprising since SP wave energy is generated relatively locally. Additionally, for buoy 51001, PNA has positive correlation with LP and negative correlation with SP, while SOI has similar, although not so significant, correlations with LP and SP cumulative winter anomalies at 51001 (Table 3). These relationships are a symptom of the very different sources of LP and SP energy at 51001, as opposed to the west coast buoys, where the signs of the correlations are the same.

[39] Persistent monthly winter LP energy anomalies at buoy 46005 occur over multiyear periods (Figure 5), e.g., negative anomalies are generally observed during the early 1980s and early 1990s while positive LP anomalies are observed during the late 1980s and over the last several years. The observed variability suggests that similar atmospheric circulation patterns can persist for several successive winters over the central North Pacific. This apparent multiyear persistence of atmospheric circulation patterns undoubtedly somewhat obscures the PC correlations with SOI and PNA.

9. Trends in Wave Energy

[40] The question of changing wave climate conditions in the northeast Pacific has been under consideration since

Table 2. Correlation Coefficients, $\mathcal{R}$, of LP, IP, and SP Winter (November–March) Principal Components, With the Winter PNA and −SOI Indices Shown in Figure 12[a]

Band	Mode	PNA (p)	−SOI (p)
LP	1	**0.63** (0.00)	0.27 (0.22)
	2	**0.42** (0.05)	**0.58** (0.00)
	3	−0.03 (0.91)	−0.10 (0.66)
IP	1	**0.59** (0.00)	0.36 (0.10)
	2	**0.66** (0.00)	**0.60** (0.00)
	3	−0.36 (0.10)	0.22 (0.33)
SP	1	**0.48** (0.02)	0.31 (0.17)
	2	**0.46** (0.03)	**0.50** (0.02)
	3	−0.15 (0.52)	0.17 (0.46)

[a]Principal components are shown in Figure 8. Values in parentheses, p, associated with the preceding $\mathcal{R}$, are t-test-derived probabilities, assuming that the data are normally distributed; p values < 0.05 indicate that the associated $\mathcal{R}$ (in boldface) is statistically significant.

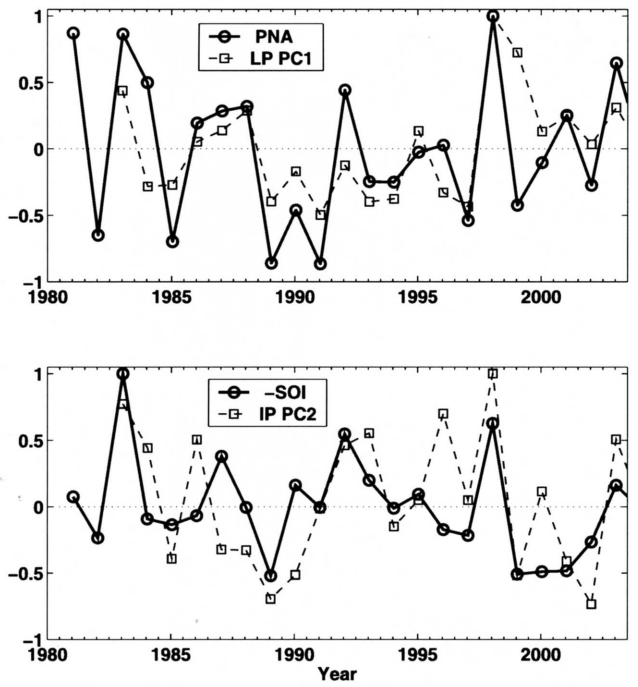

Figure 12. Demeaned, normalized cumulative winter (November–March) (top) PNA and LP PC1 and (bottom) -SOI and IP PC2. These pairs give the highest correlation coefficients $\mathcal{R}$ for PC1 and PC2 with respective indices in Table 2.

extensive damage from extreme waves occurred along the California coast during the 1982–1983 great El Niño [e.g., *Seymour et al.*, 1984; *Seymour*, 1996]. More recently, *Allan and Komar* [2000] found increasing wave heights off the Oregon-Washington coast, but decreasing wave heights off southern California, generally consistent with monthly wave energy trends shown in Figure 4. However, because the North Pacific contains substantial low-frequency variability in atmospheric circulation involving changes in pressure patterns and associated winds, and since the wave data can potentially contain significant low-frequency (decadal-scale) variability [*Graham and Diaz*, 2001; *Bromirski et al.*, 2003], the significance of any trends estimated from these relatively short time series must be considered accordingly.

[41] In contrast to the trends observed by *Allan and Komar* [2000], hindcast H_s data show greater upward trends in extreme wave heights off southern California than the Oregon-Washington coast [*Graham and Diaz*, 2001]. However, the longer-term trends in *Graham and Diaz* [2001], covering the 1948–1998 time period, should not necessarily be expected to agree with shorter-term trends during the last 20 years or so that likely include significant decadal-scale variability. Thus it appears that while the hindcast wave model H_s may provide a reasonable estimate of broad-scale trends in spatial variability of wave heights over the northeast Pacific, modeled H_s at particular locations may differ substantially with measured H_s for individual events and over a 20 year period.

[42] A change in the wave climate of the North Atlantic has been observed in the last few decades [e.g., *Bacon and Carter*, 1991; *Bouws et al.*, 1996]. The *WASA Group* [1998] reported an increase in the number of large wave episodes in the North Atlantic beginning about 1970. *Seymour* [1996] found a similar increase in extreme events from North Pacific storms affecting the southern California coast since about 1975. Thus there appears to be some evidence for recent increases in extreme wave heights (and therefore storminess) in parts of the North Atlantic as well as the North Pacific.

[43] The question of changing wave energy can also be examined from the behavior of the PCs of the leading EOFs. The least squares trend for LP PC1 is significant at the 90% confidence level (at about 80% excluding the 1997–1998 winter), suggesting that cyclone intensity (as characterized by storm size, wind speed, and duration) has been increasing in the NE Pacific since 1980, in general agreement with *Wang and Swail* [2000] and *Graham and Diaz* [2001] and confirmed by analysis of 500 hPa height variance (see Figure 13 below). The trends for IP and SP PC1 are also positive, but not strong enough to rate as statistically significant.

[44] The north-south distribution of wave energy is characterized by PC2 (Figure 8). Positive PC2 amplitudes are dominated by more southern wave energy, while negative PC2 amplitudes imply that northern wave energy dominates. Because IP and SP levels are more sensitive to local and regional storm activity than is LP energy, the generally higher IP and SP PC 2 levels in the early 1980s compared with the late 1990s indicates an increased tendency for heightened storminess in the central North Pacific, consistent with comparisons of monthly mean energy levels above and analysis of 500 hPa differences (see Figure 13 and related discussion below). The extreme positive amplitudes for IP and SP PC2 in the early 1980s also indicate that increased storminess at southern locations was more prevalent during that time. Following the convention used for mode 2, i.e., that positive mode 3 EOFs give positive principal components that are associated with southern wave energies, the strong decreasing trend in SP PC3 is also consistent with an increased tendency for somewhat more northerly storm tracks since the early 1980s.

Table 3. Correlation Coefficients, $\mathcal{R}$, of LP and SP Cumulative Winter (November–March) Anomalies, With Cumulative Winter PNA and −SOI Indices Shown in Figure 12[a]

	PNA		SOI	
Buoy	LP (p)	SP (p)	LP (p)	SP (p)
46001	0.04 (0.85)	0.06 (0.78)	−0.29 (0.17)	0.12 (0.57)
46003	−0.17 (0.40)	**−0.61** (0.00)	**−0.40** (0.05)	**−0.45** (0.03)
46005	0.23 (0.29)	0.10 (0.65)	−0.01 (0.98)	−0.20 (0.36)
46002	**0.50** (0.01)	0.22 (0.30)	0.34 (0.10)	0.20 (0.34)
46022	**0.43** (0.05)	0.30 (0.18)	0.17 (0.45)	0.29 (0.19)
46006	**0.77** (0.00)	0.32 (0.14)	**0.44** (0.04)	0.06 (0.80)
46013	**0.64** (0.00)	0.30 (0.16)	0.23 (0.29)	0.10 (0.65)
46023	**0.63** (0.00)	**0.42** (0.05)	0.34 (0.11)	**0.54** (0.01)
46025	**0.65** (0.00)	0.35 (0.11)	**0.54** (0.01)	**0.47** (0.03)
51001	**0.46** (0.03)	**−0.66** (0.00)	0.41 (0.06)	−0.19 (0.38)

[a]Anomalies are shown in Figure 8. Note that the sign is reversed for SOI so that positive correlations indicate increased wave energy during the warm phase of El Niño–Southern Oscillation. Values in parentheses, p, associated with the preceding $\mathcal{R}$, are t-test-derived probabilities, assuming that the data are normally distributed; p values < 0.05 indicate that the associated $\mathcal{R}$ (in boldface) is statistically significant.

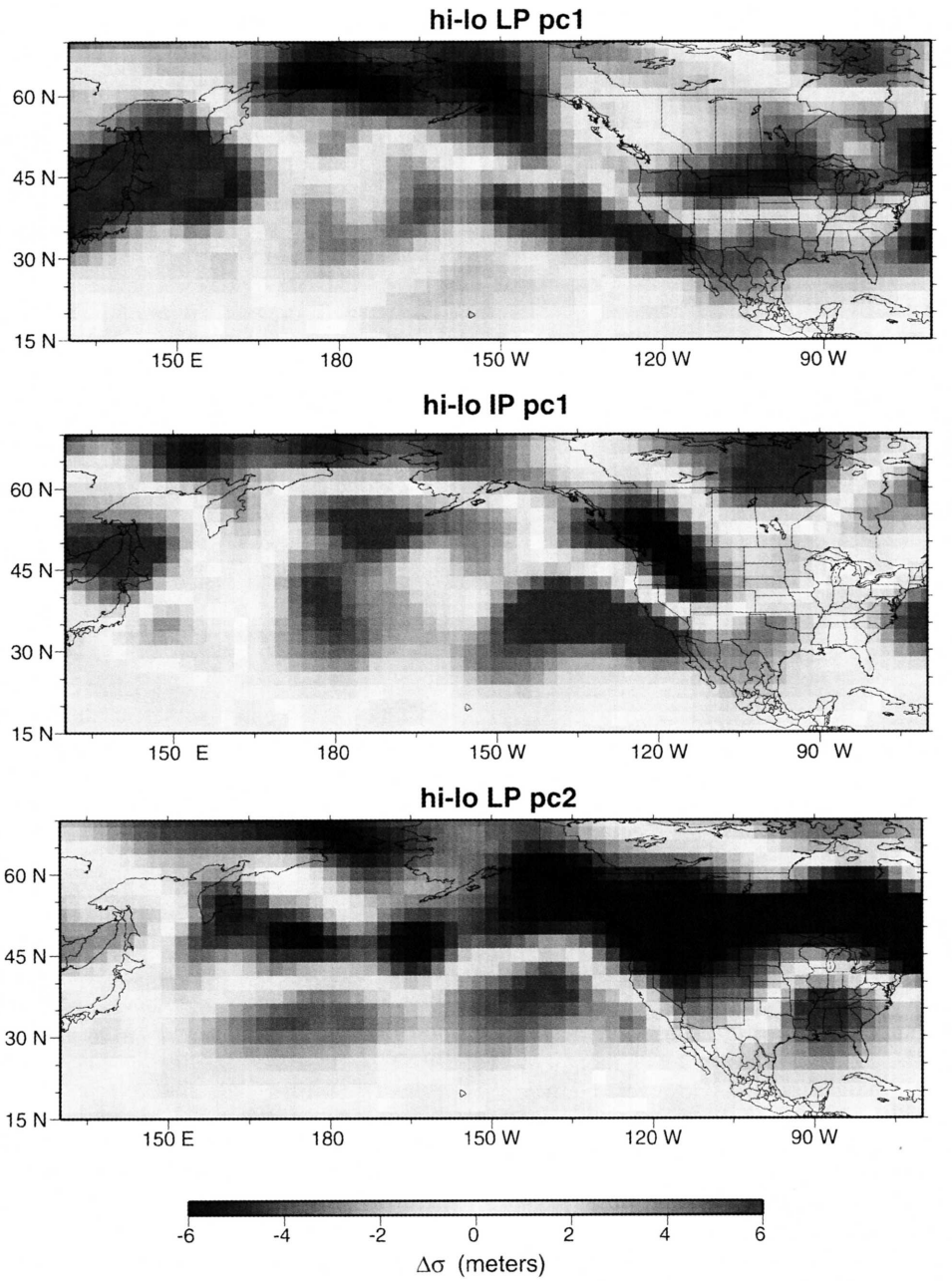

Figure 13. Difference in storm activity associated with months of high versus low amplitudes of LP and IP PCs. Maps show differences between composites of the standard deviation ($\Delta\sigma$) of 3–10 day band-passed 500 hPa heights. Composites were formed from months with the 10 highest and 10 lowest amplitudes of each PC. Positive $\Delta\sigma$ implies increasing storminess. See color version of this figure at back of this issue.

[45] Further insight into trends in wave energy over the period of the buoy record can be obtained by an examination of associated storminess in the NE Pacific. Different patterns of atmospheric circulation, as represented by the 700 hPa height anomaly patterns in Figures 9–11, should be associated with distinctive patterns of storminess. The spatial and secular distribution of wave energy levels is thus directly related to cyclone frequency, intensity, and location, i.e., storminess. Storminess was estimated from the monthly standard deviation of [3,10] day band-pass-filtered NCEP reanalysis 500 hPa height data as described by *Dettinger et al.* [2001]. To emphasize the location of intense cyclonic variability and establish the association between storminess and wave energy variability, differences ($\Delta\sigma$) were obtained between composites of the filtered 500 hPa height storminess data for groups of months containing the 10 highest and 10 lowest PCs for LP and IP energy shown in Figure 8.

[46] As discussed above, high LP wave energy levels result from large, intense storms that often have a basin-wide impact, while IP levels have more regional forcing. Thus the LP PC1 storminess composite (Figure 13 (top))

indicates that extreme storm activity is concentrated in the central North Pacific, in agreement with *Graham and Diaz* [2001], the above analyses of monthly wave energy and wind speed (Figures 4 and 6, respectively), and the SP PC2 700 hPa height anomaly composite (Figure 11). The storminess composite associated with IP PC1 (Figure 13 (middle)) indicates a more regionally concentrated area of storminess across much of the North Pacific, although there is a more distant region of storminess centered at about 180°W that is teleconnected with the West Coast pattern. These patterns are consistent with the broad regional extent of mode 1 variability indicated by IP EOF 1 and its associated 700 hPa height composite (Figures 7 and 9, respectively). Similarly, the north-south pattern of storminess variability (Figure 13 (bottom)) follows the spatial distribution of wave energy indicated by wave energy EOF 2. The pattern for IP PC2 is consistent with increased storminess in the south during El Niño and in the north during La Niña. A southward shift in storminess during the El Niño phase of ENSO is particularly noticeable in the storminess difference map for IP PC2 (Figure 13 (bottom)), in that IP PC2 high positive amplitudes are quite well correlated with El Niño (−SOI) events (Table 2).

[47] Note that concentrations of strong variability are located about equidistant from the Oregon-Washington coast for both positive and negative $\Delta\sigma$ in the PC2 composite, and also relatively near the Oregon-Washington coast for positive $\Delta\sigma$ in both LP and IP PC1 composites. When considered in conjunction with increasing storm intensity indicated by the upward trend in LP PC1 (Figure 8), proximity to these concentrations of strong variability may explain the increase in wave height observed by *Allan and Komar* [2000] at buoy 46005 and probably at other coastal locations, consistent with conclusions from trends in monthly wave energy discussed above. An additional feature of the IP PC2 composite is the continuation of the strong negative $\Delta\sigma$ pattern over North America, indicating the importance of storm variability across the eastern North Pacific to weather patterns across the northern United States.

[48] The impact of regional storm variability shown in Figure 13 is reflected in the number of extreme IP and SP events during El Niño/La Niña episodes. Extreme event thresholds were determined for all available hourly IP and SP data at the 98% level at representative buoys. Recognizing the small number of strong ENSO related events and that the Northern Hemisphere's response to ENSO is spatially variable [*Gershunov and Barnett*, 1998], we consider the two northern buoys (46001 and 46005, see Figure 1) and the two southern buoys (46023 and 46025) together. In general, more extreme IP and SP events occur at the southern buoys during El Niño and at the northern buoys during La Niña (Figure 14), although the El Niño relationship at southern locations is stronger and neutral winters can also exhibit high wave energy. Scatter plots (not shown) of monthly SOI versus the wave energy PC amplitudes associated with correlations shown in Tables 2 and 3, indicate that there is considerable scatter in this relationship, but do not reveal any obvious nonlinearities. Comparing the frequency of extreme IP and SP events at 46005 also suggests that these wave energy components can vary somewhat independently, e.g., there were more IP than SP

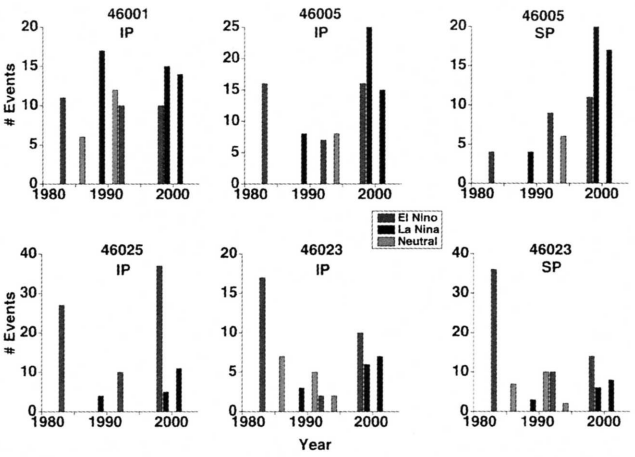

Figure 14. Number of extreme events of IP and SP wave energy during winter months (December–March) during strong El Niño (red, 1982–1983, 1991–1992, and 1997–1998), strong La Niña (blue, 1988–1989, 1998–1999, and 2000–2001), and ENSO neutral (cyan, 1985–1986, 1990–1991, and 1993–1994) winters (see Figure 12) at northern buoys 46001 and 46005 and at southern buoys 46025 and 46023. An included event exceeds the 98th percentile energy level for at least 3 hours. The four panels on the left show extreme IP event frequencies, while the two panels on the right reflect extreme SP events. See color version of this figure at back of this issue.

extreme events during the 1982–1983 El Niño. The opposing shifts in the frequency of SP extremes over time at the two locations is consistent with an increased tendency for somewhat more northerly storm activity in the coastal and near-coastal environment since the early 1980s. These shifts are indicated by the trends in SP wave energy at 46023 and 46005 and the pattern in $\Delta\sigma$ for IP PC1 (Figure 13) that reflects the differences in storminess associated with times of high versus low IP PC1, the high values occurring more frequently since 1995.

10. Conclusions

[49] A 23 year record (1981–2003) of surface gravity wave energy recorded by ten NOAA wave and meteorological buoys in the NE Pacific reveals that wave activity, which varies considerably from month to month and year to year, is organized coherently over regional to basin spatial scales. The wave energy can fluctuate by as much as a factor of five or more at individual buoys from year to year. Wave energy variability in the northeast Pacific is closely related to broad-scale atmospheric circulation modes that affect climate variability across the North Pacific and North America. Three separate frequency bands corresponding to long periods (LP), intermediate periods (IP), and short periods (SP), were investigated, revealing rather similar spatial structure and temporal variability. Using principal component analysis, the dominant mode of wave energy is seen to have a nearly basin-wide influence, while the second mode shows a distinct north-south spatial pattern that is related to southward or northward migrations of the North Pacific storm track in association with the El Niño-Southern Oscillation (ENSO) phenomenon.

[50] Although relatively high, positive correlations are obtained between principal components across LP and IP wave frequency bands, somewhat different atmospheric anomaly composites associated with PC extremes are obtained, indicating that wave energy is quite sensitive to the placement of anomaly centers and their associated storminess. Because large-scale monthly atmospheric patterns (such as PNA and SOI) produce swarms of storms and high winds over broad, unfocused regions of the northeast Pacific, their correlations with discrete buoy records or with collective wave energy PC time series are somewhat degraded. The PNA pattern produced the strongest correlations with individual buoy wave energy and with the first two LP, IP, and SP EOF modes. In contrast to PNA, correlations of SOI with PC1 (that dominates the variance explained) are weak (see Table 2), indicating that ENSO does not much explain the trends observed in wave energy. Correlations of SOI with wave energy at individual buoys are also generally weak or only moderately strong (see Table 3). Thus while ENSO plays a significant role in the distribution of wave energy, as indicated by the relatively good correlations of PC2 with SOI shown in Table 2 and atmospheric anomaly composites, ENSO's influence on observed trends in wave energy is not strong.

[51] High correlations of monthly anomalies between the buoys confirms the basin-wide impact of LP wave energy, while weaker correlations between SP wave energy anomalies demonstrate the more regional extent of higher-frequency gravity waves. An increasing trend in the principal components associated with the dominant EOF mode of LP energy suggests that storminess has increased in the northeast Pacific since 1980, in agreement with increasing trends in cyclone intensity [*Graham and Diaz*, 2001]. The inferred tendency of a more northerly concentration of storm activity in the central North Pacific may indicate a broad-scale change in atmospheric circulation patterns that would have significant implications for coastal erosion in the Pacific Northwest as well as the potential for drought in the southwestern United States.

[52] Monthly means of wave spectral energy and their principal components indicate that the 1997–1998 El Niño winter produced the highest basin-wide energy in the available buoy record, followed by another high wave energy episode during the 1982–1983 El Niño. During El Niño, patterns of storminess variability are consistent with increasing activity in the central North Pacific, as well as the tendency for more extreme waves in the south. During La Niña, wave energy is generally elevated in the north. However, the buoy data set is rather short, and much longer-term measures such as PDO and the *Bromirski et al.* [2003] San Francisco tide gauge storminess index show pronounced interdecadal variability, suggesting that storm activity comparable to recent levels previously occurred in epochs prior to 1950. Reconstructions of the wave heights from microseismic data [*Bromirski et al.*, 1999] during El Niños in earlier epochs, e.g., the strong 1940–1941 El Niño, could help clarify whether the apparent recent intensification of wave energy is exceptional.

[53] Positive correlations between LP and SP wave energy have important implications because the same local storms that produce high SP wave energy usually involve low atmospheric pressure which creates heightened sea levels due to an inverse barometer effect. When these high sea levels are accompanied by large swell (i.e., high LP energy), coastal regions are more vulnerable to flooding and erosion. Cases such as 1982–1983, which contained a mixture of high swell and local storminess that occurred during high astronomical tides, were especially damaging to structures and real estate along the California coast. The increase in LP wave energy observed since 1980 is consistent with an increasing trend in a central California tide gauge storminess index over the past 50 years [*Bromirski et al.*, 2003]. The coincidence of extreme wave episodes and high storm surge, combined with rising sea level and increasing tide ranges along much of the West Coast [*Flick et al.*, 2003], increases the likelihood that more wave energy will reach exposed beaches, sea cliffs, coastal developments, and other vulnerable coastal assets.

[54] **Acknowledgments.** This work was supported by the California Department of Boating and Waterways as part of their program to improve boating facilities, access, safety, and education, the NOAA Office of Global Programs through the California Applications Program, the Department of Energy, and the California Energy Commission through the California Climate Change Center. Thanks to Emelia Bainto and Mary Tyree for analyses and graphics. We thank Nick Graham for useful discussions and Mike Dettinger for use of grid filtering codes to generate storminess data.

References

Allan, J., and P. D. Komar (2000), Are ocean wave heights increasing in the eastern North Pacific?, *Eos Trans. AGU*, *81*, 561–567.

Armstrong, G., and R. E. Flick (1989), Storm damage assessment for the January 1988 storm along the southern California shoreline, *Shore Beach*, *57*, 18–23.

Bacon, S., and D. J. T. Carter (1991), Wave climate changes in the North Atlantic and North Sea, *Int. J. Climatol.*, *11*, 545–558.

Barnston, A. G., and R. E. Livezey (1987), Classification, seasonality and persistence of low-frequency atmospheric circulation patterns, *Mon. Weather Rev.*, *115*, 1825–1850.

Bjerknes, J. (1966), A possible response of the atmospheric Hadley circulation to equatorial anomalies of ocean temperature, *Tellus*, *18*, 820–829.

Bjerknes, J. (1969), Atmospheric teleconnections from the tropical Pacific, *Mon. Weather Rev.*, *97*, 163–172.

Bouws, E., D. Jannick, and G. J. Komen (1996), The increasing wave height in the north Atlantic Ocean, *Bull. Am. Meteorol. Soc.*, *77*, 2275–2277.

Bromirski, P. D., R. E. Flick, and N. Graham (1999), Ocean wave height from inland seismometer data: Implications for investigating wave climate changes in the NE Pacific, *J. Geophys. Res.*, *104*, 20,753–20,766.

Bromirski, P. D., R. E. Flick, and D. R. Cayan (2003), Storminess variability along the California coast: 1858–2000, *J. Clim.*, *16*, 982–993.

Cayan, D. R., K. T. Redmond, and L. G. Riddle (1999), ENSO and hydrologic extremes in the western United States, *J. Clim.*, *12*, 2881–2893.

Dettinger, M. D., D. S. Battisti, R. D. Garreaud, G. J. McCabe, and C. M. Bitz (2001), Interhemispheric effects of interannual and decadal ENSO-like climate variations on the Americas, in *Interhemispheric Climate Linkages: Present and Past Climates in the Americas and Their Societal Effects*, edited by V. Markgraf, pp. 1–16, Elsevier, New York.

Dole, R. M. (1986), Persistent anomalies of the extratropical Northern Hemisphere wintertime circulation: Structure, *Mon. Weather Rev.*, *114*, 178–207.

Earle, M. D., K. E. Steele, and Y.-H. Hsu (1984), Wave spectral corrections for measurements with hull-fixed accelerometers, *Proc. Oceans*, *84*, 725–730.

Flick, R. E., J. F. Murray, and L. C. Ewing (2003), Trends in United States tidal datum statistics and tide range, *J. Waterw. Port Coastal Ocean Eng.*, *129*, 155–164.

Gershunov, A., and T. P. Barnett (1998), Interdecadal modulation of ENSO teleconnections, *Bull. Am. Meteorol. Soc.*, *79*, 2715–2725.

Graham, N. E., and H. F. Diaz (2001), Evidence for intensification of North Pacific winter cyclones since 1948, *Bull. Am. Meteorol. Soc.*, *82*, 11,869–11,893.

Hoerling, M. P., and A. Kumar (2002), Atmospheric response patterns associated with tropical forcing, *J. Clim.*, *15*, 2184–2203.

Horel, J. D., and J. M. Wallace (1981), Planetary-scale atmospheric phenomena associated with Southern Oscillation, *Mon. Weather Rev.*, *109*, 813–829.

Inman, D. L., and P. M. Masters (1991), Budget of sediment and prediction of the future state of the coast, in *Coast of California Storm and Tidal Waves Study*, vol. 1, *State of the Coast Report, San Diego Region*, chap. 9, pp. 1–105, U.S. Army Corps of Eng. Los Angeles Dist., Calif.

Mantua, N. J., S. R. Hare, Y. Zhang, J. M. Wallace, and R. C. Francis (1997), A Pacific interdecadal climate oscillation with impacts on salmon production, *Bull. Am. Meteorol. Soc.*, *78*, 1069–1079.

Mo, K. C., and R. E. Livezey (1986), Tropical-extratropical geopotential height teleconnections during the Northern Hemisphere winter, *Mon. Weather Rev.*, *114*, 2488–2515.

Namias, J. (1968), The labile Gulf of Alaska cyclone—Key to large scale weather modification elsewhere, paper presented at the International Conference on Cloud Physics, Toronto, Canada.

Namias, J. (1976), Some statistical and synoptic characteristics associated with El Niño, *J. Phys. Oceanogr.*, *6*, 130–138.

Namias, J. (1978), Multiple causes of the North American abnormal winter 1976–77, *Mon. Weather Rev.*, *106*, 279–295.

Nitta, T., and S. Yamada (1989), Recent warming of tropical sea surface temperatures and its relationship to the Northern Hemisphere circulation, *J. Meteorol. Soc. Jpn.*, *67*, 375–383.

Seymour, R. J. (1996), Wave climate variability in southern California, *J. Waterw. Port Coastal Ocean Eng.*, *122*, 182–186.

Seymour, R. J., R. R. Strange III, D. R. Cayan, and R. A. Nathan (1984), Influence of El Niños on California's wave climate, in *Nineteenth Coastal Engineering Conference, Proceedings of the International Conference, September 3–7, 1984, Houston, Texas*, edited by B. L. Edge, pp. 577–592, Am. Soc. of Civ. Eng., New York.

Steele, K. E., J. C. Lau, and Y. L. Hsu (1985), Theory and application of calibration techniques for an NDBC directional wave measurements buoy, *IEEE J. Oceanic Eng.*, *10*, 382–396.

Trenberth, K. E., and J. W. Hurrell (1994), Decadal atmosphere-ocean variations in the Pacific, *Clim. Dyn.*, *9*, 303–319.

Wallace, J. M., and D. S. Gutzler (1981), Teleconnections in the geopotential height field during the Northern Hemisphere winter, *Mon. Weather Rev.*, *109*, 784–812.

Wang, X. L., and V. R. Swail (2000), Changes in extreme wave heights in Northern Hemisphere oceans and related atmospheric regimes, *J. Clim.*, *14*, 2204–2221.

WASA Group (1998), Changing waves and storms in the northeast Atlantic, *Bull. Am. Meteorol. Soc.*, *79*, 741–761.

P. D. Bromirski and R. E. Flick, Integrative Oceanography Division, 0209, Scripps Institution of Oceanography, University of California, San Diego, 9500 Gilman Drive, La Jolla, CA 92093-0209, USA. (pbromirski@ucsd.edu; ref@coast.ucsd.edu)

D. R. Cayan, Climate Research Division, 0224, Scripps Institution of Oceanography, University of California, San Diego, 9500 Gilman Drive, La Jolla, CA 92093-0224, USA. (dcayan@ucsd.edu)

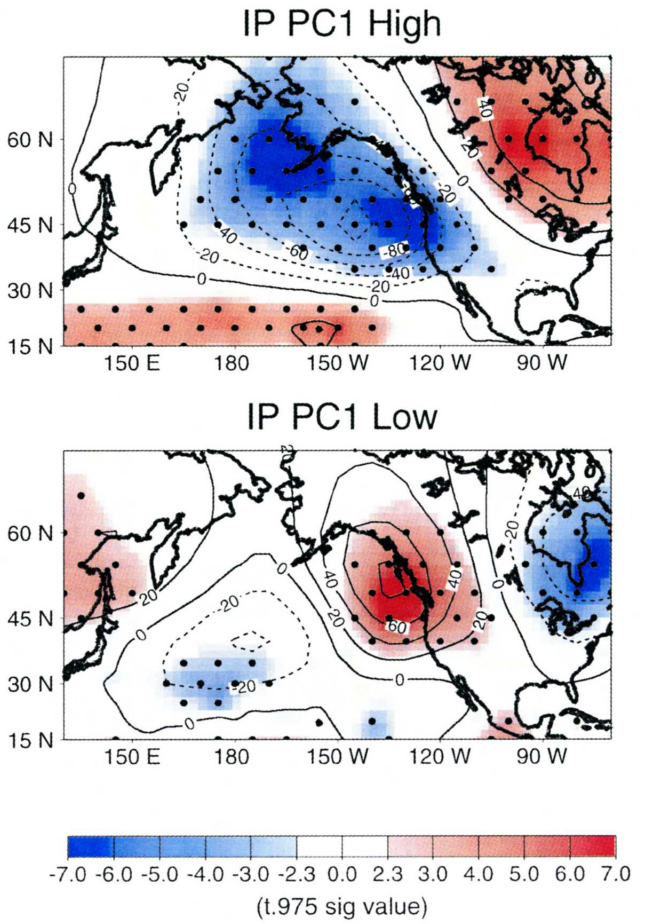

Figure 9. Composite 700 hPa height anomalies for months with the (top) 10 highest and the (bottom) 10 lowest IP principle component (PC) mode 1 extremes (see Figure 8). Strong negative anomalies associated with deep negative anomaly patterns are blue, while strong positive anomalies are red.

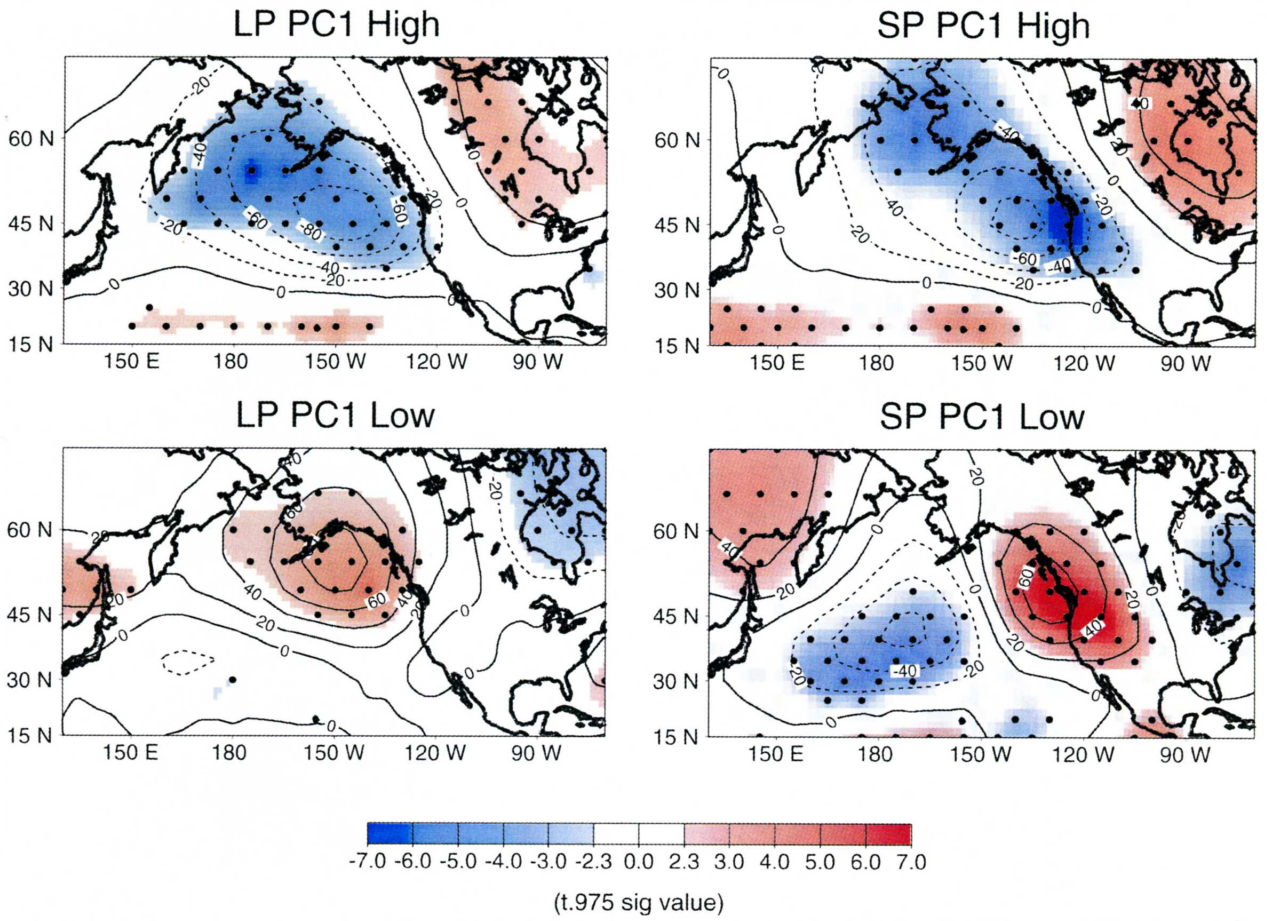

Figure 10. Composite 700 hPa height anomalies for months with the (top) 10 highest and the (bottom) 10 lowest (left) LP and (right) SP principle component (PC) mode 1 extremes (see Figure 8). Strong negative anomalies associated with deep low negative patterns are blue, while strong positive anomalies are red.

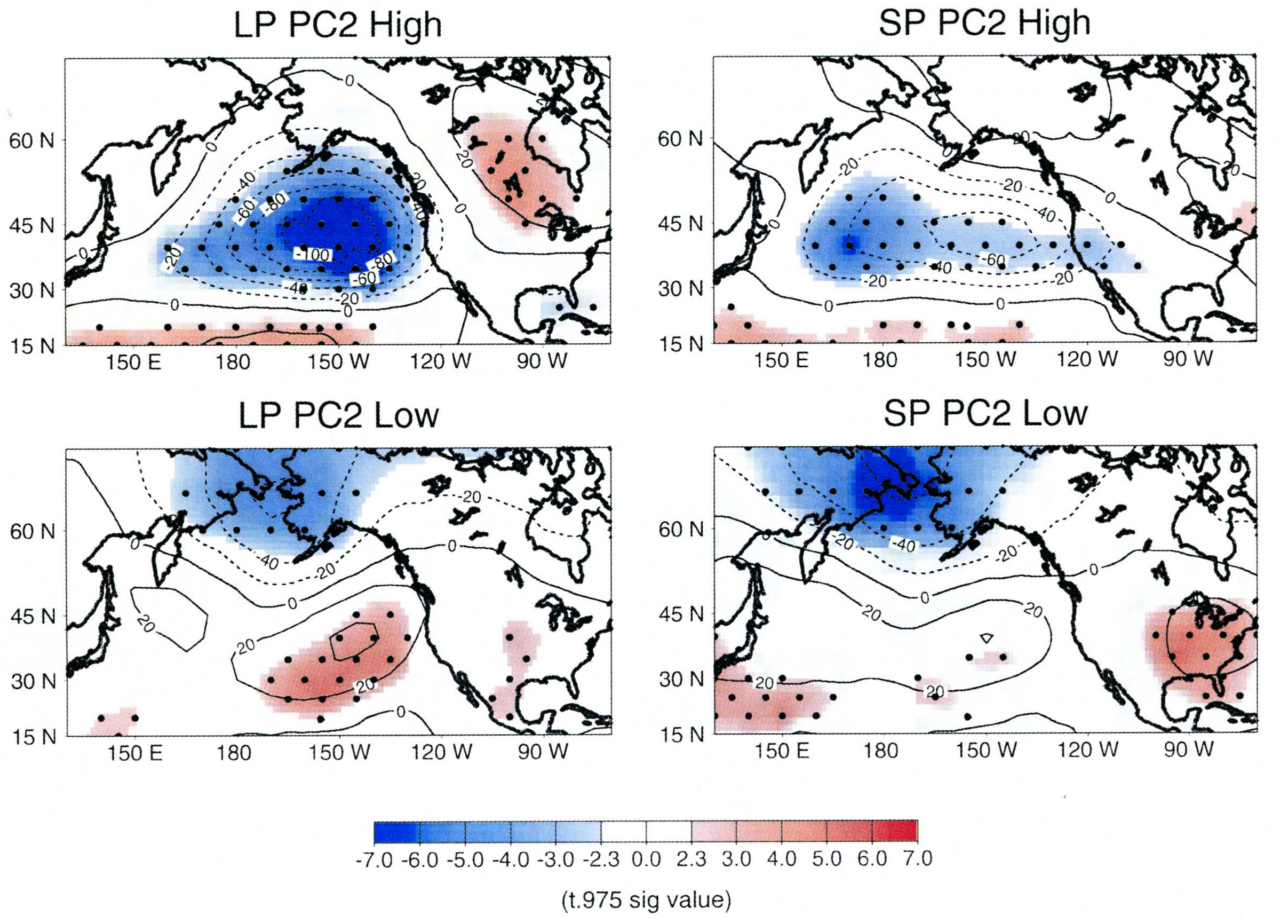

Figure 11. Composite 700 hPa height anomalies for months with the (top) 10 highest and the (bottom) 10 lowest (left) LP and (right) SP principle component (PC) mode 2 extremes (see Figure 8). Strong negative anomalies associated with deep low negative patterns are blue, while strong positive anomalies are red.

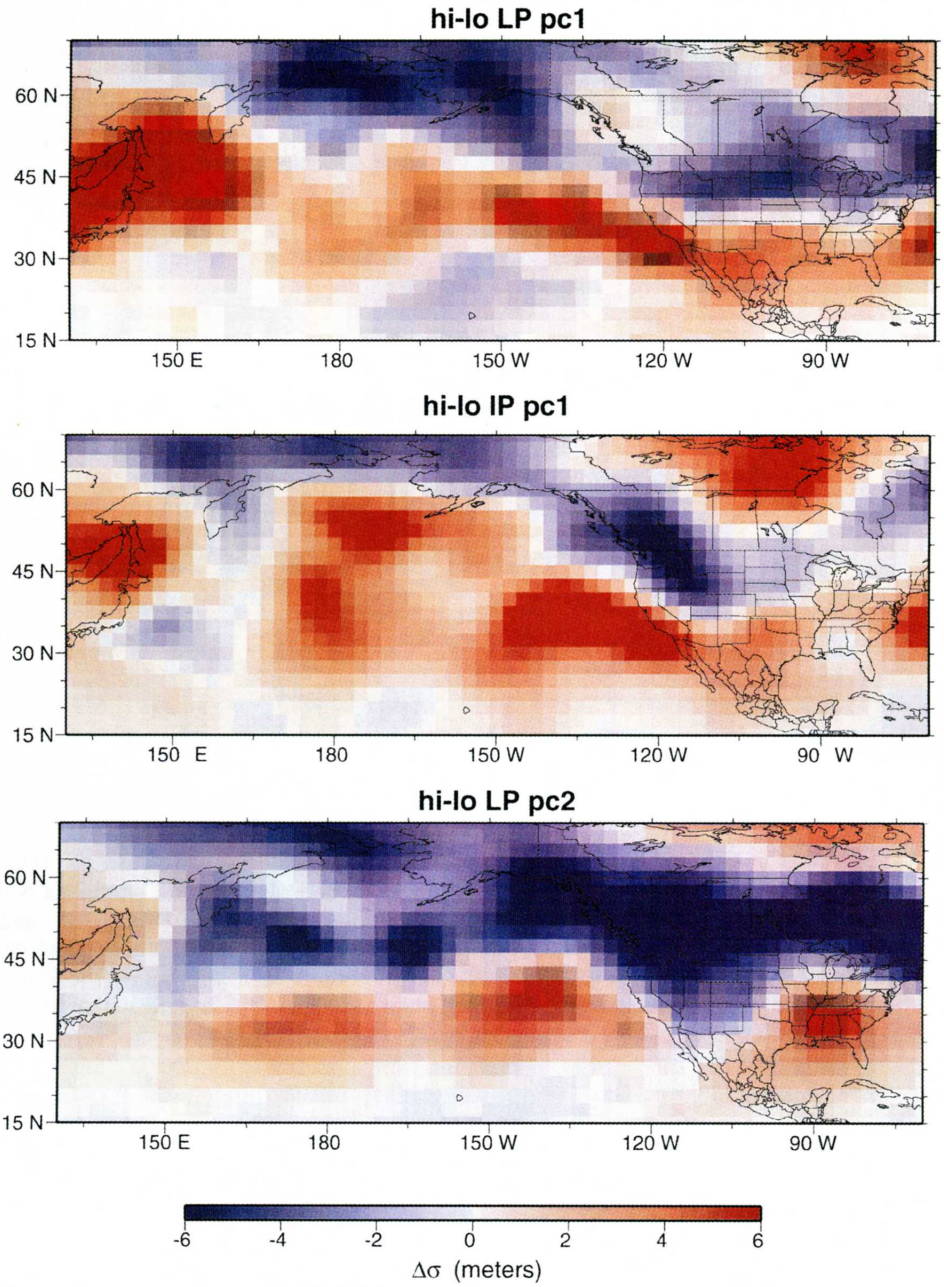

Figure 13. Difference in storm activity associated with months of high versus low amplitudes of LP and IP PCs. Maps show differences between composites of the standard deviation ($\Delta\sigma$) of 3–10 day band-passed 500 hPa heights. Composites were formed for months with the 10 highest and 10 lowest amplitudes of each PC. Positive $\Delta\sigma$ implies increasing storminess.

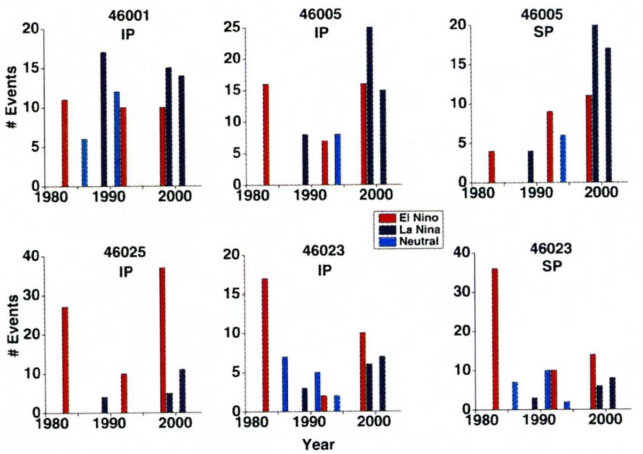

Figure 14. Number of extreme events of IP and SP wave energy during winter months (December–March) during strong El Niño (red, 1982–1983, 1991–1992, and 1997–1998), strong La Niña (blue, 1988–1989, 1998–1999, and 2000–2001), and neutral (cyan, 1985–1986, 1990–1991, and 1993–1994) SOI winters (see Figure 12) at northern buoys 46001 and 46005 and at southern buoys 46025 and 46023. An included event exceeds the 98th percentile energy level for at least 3 hours. The four panels on the left show extreme IP event frequencies, while the two panels on the right reflect extreme SP events.